Characterization of insulators by high-resolution electron-energy-loss spectroscopy: Application of a surface-potential stabilization technique

M. Liehr,* P. A. Thiry, J. J. Pireaux, and R. Caudano
Laboratoire de Spectroscopie Electronique, Institut de Recherche sur les Interfaces Solides, Facultés Universitaires Notre-Dame de la Paix, 61 rue de Bruxelles, B-5000 Namur, Belgium
(Received 9 December 1985)

A surface-potential stabilization technique is described which permits one to take vibrational spectra of excellent quality with high-resolution electron-energy-loss spectroscopy on insulating samples of very different types, such as ionic insulators and polymers. Induced surface conductivity and enhanced secondary-electron emission close to the vacuum level are found to be at the origin of the surface-potential stabilization, which is done by irradiation of the sample with electrons in the keV range. Nonequilibrium carrier densities and mean free paths are estimated from observable Drude damping. Irradiation effects are discussed.

INTRODUCTION

Most analytical techniques for surface characterization either involve interaction of a sample with a beam of charged particles, such as in Auger-electron spectroscopy (AES), ion scattering spectrometry (ISS), secondary-ion mass spectrometry (SIMS), or electron-energy-loss spectroscopy (EELS), or they involve the emission of charged particles, e.g., in the case of x-ray or uv photoelectron spectroscopy (XPS-UPS). Insulators cause crucial problems to all these methods[1] because charge buildup can occur due to captured or emitted electrons or ions. These complications inherent to insulators have severely limited the number of scientific results obtained on insulator surfaces when compared to semiconductors and metals.

Several "standard" methods, each specially adapted to one single-surface analytical technique, have evolved to deal with this problem. Methods involving the deposition of a metallic grid[2] risk surface contamination; heating[3] to increase the bulk conductivity may lead to ionic conduction and consequent decomposition of the sample as well as degradation of the spectra.[4] Frequently, charge compensation is achieved by flooding the sample with carriers of the suitable polarity.[1] In this paper a method derived from this "flood gun" technique applied to EELS is described. During the last 15 years high-resolution electron-energy-loss spectroscopy (HREELS) has developed into a valuable tool in surface physics like, e.g., for species identification in heterogeneous catalysis or characterization of surface elementary excitations and their interactions.[5,6] Until recently a major shortcoming of HREELS was its limited applicability to materials with vanishing bulk and surface conductivities.

A method to stabilize the surface potential of various kinds of insulators has been presented[7] and applied to different wide-band-gap insulators.[8,9] It consists in irradiation of the sample surface with an auxiliary electron beam, which is provided by a standard Auger-electron spectrometer gun, thus making the method easily adaptable to any existing HREEL system. One intention of this paper is to better characterize the potential stabilization mechanisms, their limitations, and shortcomings, to provide the basis for further applications.

The potentiality of HREELS applied to insulators will be pointed out on several occasions. Dielectric functions and infrared optical constants can be derived with almost the same accuracy as done by infrared spectroscopy, offering the supplementary advantage to observe surface influences.[7] Angle-resolved secondary-electron distribution measurements allow precise determination of electronic structure and charging state of the samples. HREELS is furthermore potentially capable of deriving information about nonequilibrium carriers in insulators.

This paper will be organized into several sections. Section I describes the experimental setup, gives examples of the quality of the measured vibrational HREEL spectra, and points out which information can be extracted from them, e.g., infrared optical constants. Evaluation of sample work function and distributions of the secondary-electron background created by the potential stabilization technique are discussed in Sec. II. The precise determination of the charging state of insulator surfaces and the physical origin of the surface-potential stabilization mechanism will be dealt with in Sec. III. The influence of this method on the accurate determination of physical parameters, like cross sections, and estimated hot carriers density, mobility, and mean free path are given in Sec. IV. Section V points out to which extent defect creation due to high-energy electron irradiation can be detected.

I. SURFACE-POTENTIAL STABILIZATION: EXPERIMENT AND EXAMPLES

A. Experiment

Details of the experimental setup that allows the measurement of HREEL spectra on insulators are shown schematically in Fig. 1. The HREELS system used is a hemispherical spectrometer (type SEDRA ISA-RIBER). The analyzer can be rotated in a sector of 122° in the plane of incidence of the monochromatic electron beam. The resolution limit of the spectrometer is in the range of

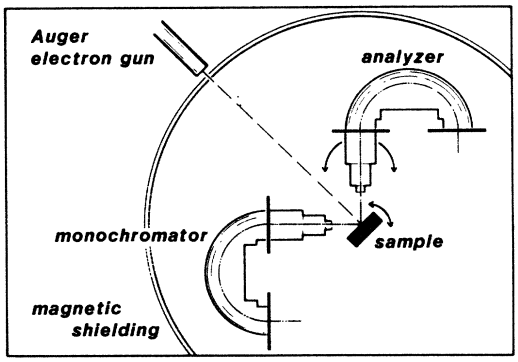

FIG. 1. Experimental setup to measure high-resolution electron-energy-loss spectra on insulator samples. In addition to the monochromatic beam an electron beam with about 1 keV and 1 μA irradiates the surface.

3 meV (25 cm^{-1}). Charging effects on insulating samples are eliminated by illuminating the material with the defocused beam of an auxiliary electron gun (CER 306, RIBER) working in the ranges of energy and current of a typical Auger spectrometer electron gun. This electron gun is mounted outside the magnetic shields around the HREEL spectrometer, and rotation of the sample allows irradiation of the target surface from near glancing to normal incidences. The probes are held by tungsten clamps which touch their surface and press the sample against a stainless-steel sample holder, which is electrically grounded. Sample anneal is performed by thermal radiation or electron bombardment from the sample backside. To initiate the neutralization, the electron beam of this auxiliary gun is first focused and centered on the sample. The exact position of the beam can be observed visually on most insulator samples because irradiation with fast electrons induces fluorescence in the visible range. Typical parameters of the auxiliary beam during this procedure are 1.5 keV energy and up to 10 μA emission current. After positioning, the beam is completely defocused and its current is reduced to a minimum to prevent extensive heating or excessive radiation damage. In this configuration, the auxiliary electron beam illuminates the whole sample area with its clamp assembly and part of the sample holder. Typical beam currents for continuous operation range from 100 nA to 1 μA. Sample surface temperature can be monitored easily with the HREEL spectrometer by measuring the intensity ratio of energy gains to losses corresponding to the same vibration. This ratio is governed by the Boltzmann factor. Typical surface temperatures never exceeded the range of 50—80 °C with the sample holder at room temperature.

Sample preparation consisted in cleaving or polishing the insulator single crystals in air followed by a thermal anneal *in situ*. The occurrence of low-energy electron-diffraction (LEED) pattern and the absence of contaminations in AES as well as the absence of CH and OH vibrational bands in HREELS were taken as signs of a good surface quality. Due to the extremely low sticking coefficients for most gases on insulators the samples remained clean by the above standards even after prolonged measurements under UHV conditions (4×10^{-11} Torr base pressure). If necessary, cleaning could be easily performed by rather mild anneals to about 900 K for 30 min. Polyethylene samples (Solvay Co., model No. DND 175) were used. No *in situ* cleaning was applied to the polymer samples.[10]

B. HREELS vibrational spectra

The high quality of the spectra obtained with this setup on anorganic ionic insulator single crystals has been demonstrated for several wide-band-gap materials like Al_2O_3,[7] MgO,[8] SiO_2,[9] LiF,[11] and NaCl.[11] Examples of spectra taken in specular reflection for MgO(001) and Al_2O_3(0001) are displayed in Figs. 2 and 3, respectively. An ultimate resolution of about 20 cm^{-1} (2.5 meV) corre-

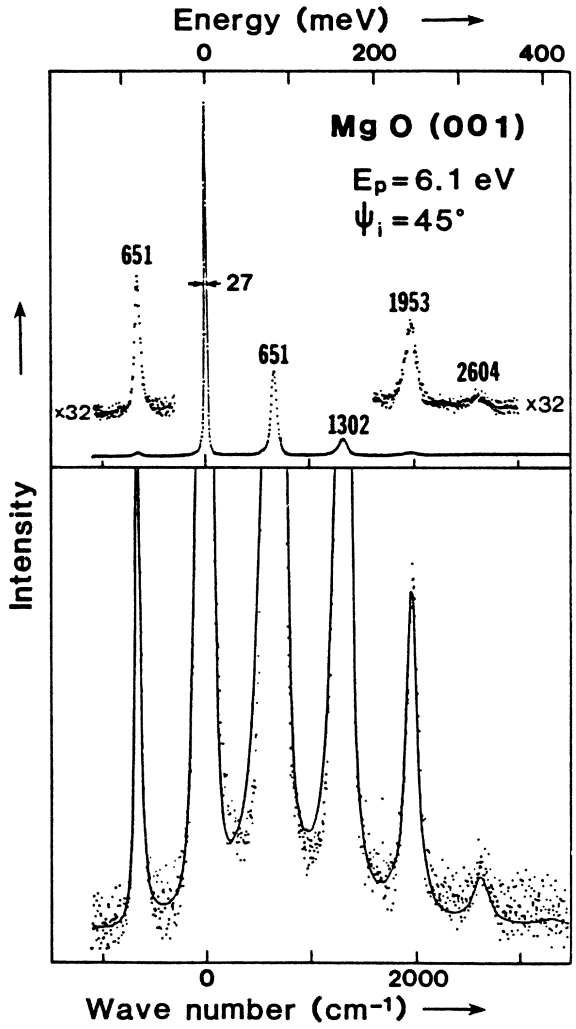

FIG. 2. Energy-loss spectrum of 6.1 eV electrons after reflection on a MgO(001) surface. The lower part shows the same spectrum on an extended scale. A fit using the dielectric theory is superposed (Ref. 8).

sponding to the resolution limit of the spectrometer was obtained on Al_2O_3. With the best adjustment the only negative influence of the auxiliary beam consisted in causing an almost linear background of rather low intensity which could easily be subtracted for data analysis. The spectra represent the elastically reflected beam and a multitude of energy gains and losses corresponding to the annihilation or excitation of so-called Fuchs-Kliewer optical surface phonons. Such phonons exist only in polar semiconductors or ionic insulators and are oscillations of the ionic sublattices of the crystal around the surface. They produce a long-range electric field that extends into the bulk and into the vacuum and couples to the electric field of the incoming probing electron. These phonon modes dominate the energy-loss spectra measured by HREELS (Ref. 12) on infrared active materials. The characteristics of Fuchs-Kliewer phonons are mainly determined by bulk properties because they extend quite far into the crystal (in the order of 10—100 nm). Nevertheless, influences of the surface are easily detectable with the high resolution achieved with the neutralization technique. Such influences are supplementary deexcitation channels for the surface phonons such as surface irregularities[11] and surface states[7] which tend to broaden the phonon loss lines, or additional vibrations localized at defects. As in infrared (ir) spectroscopy, anharmonicity effects and anisotropic optical constants can be detected.

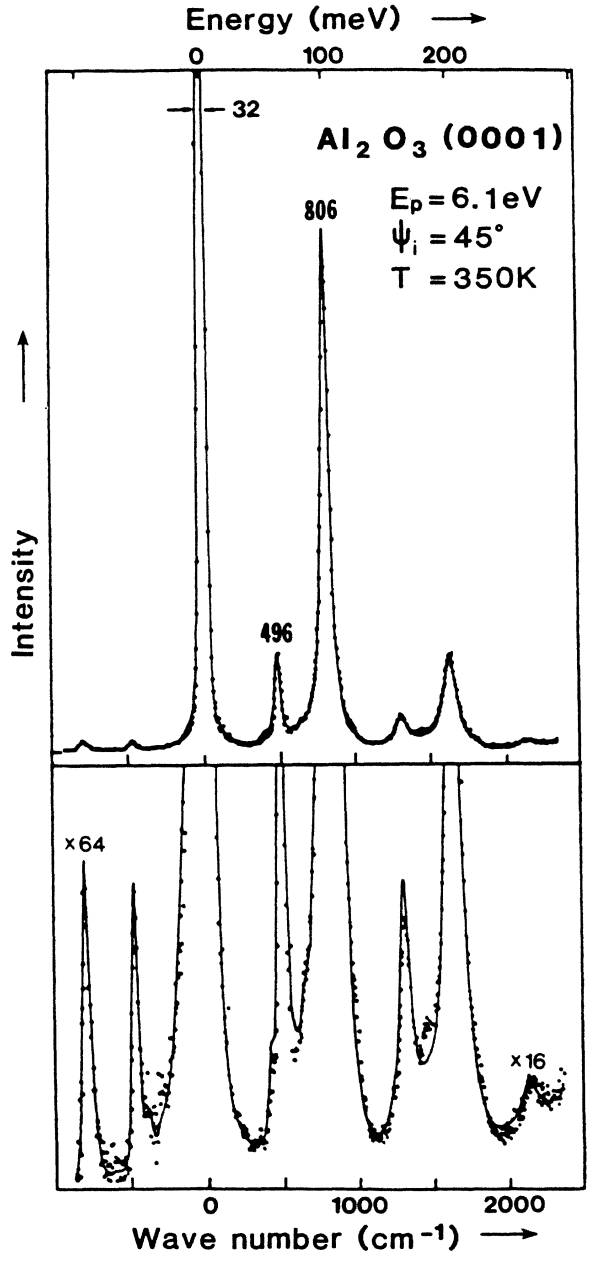

FIG. 3. Energy-loss spectrum of 6.1 eV electrons after reflection on a Al_2O_3(0001) surface exhibiting a nonprimitive LEED pattern. The elastic peak is about 4 times larger than the strongest loss. A fit to the spectrum is superposed (Ref. 7). The lower part shows the same spectrum on an extended scale.

Fuchs-Kliewer phonon spectra have been described theoretically by the so-called dielectric theory,[13] which has recently been extended to optically anisotropic materials like Al_2O_3.[14] The accuracy of this theoretical approach could be demonstrated in a spectacular way by comparison with experimental data for MgO (Ref. 8) and Al_2O_3 (Ref. 7). The semiclassical approach used by this theory has been justified by a fully quantum-mechanical treatment yielding the same results.[15] Our data analysis consisted in numerical calculations of the "classical" loss function $P_{cl}(\hbar\omega)$ derived from the dielectric theory to simulate the experimental spectra and to extract infrared optical constants with about the same accuracy as with ir spectroscopy. The quality of the numerical simulations can be judged by comparing experiment and fit for MgO and Al_2O_3 (Figs. 2 and 3). Details about the theoretical models and the data processing have been published elsewhere.[7,8] A further development of the underlying theory also permits us to study multilayered systems.[9] As has been demonstrated, this surface-potential stabilization technique is not restricted to single-crystal substrates but has been successfully applied to amorphous films, to thin-film interfaces,[16] and to polymer surfaces.[10] It therefore eliminates completely the restriction believed to exist for the application of high-resolution EELS to all nonconducting materials. A spectrum of a thick polymer sample (polyethylene) is shown in Fig. 4 as an example of a pseudocrystalline organic material. Despite the very different nature of the material, spectra with sufficient resolution can be obtained [70—120 cm^{-1} full width at half maximum (FWHM)]. Currents and voltages of the auxiliary and primary electron guns can be chosen in a way to minimize surface decomposition of the sample (Sec. V). The surface potential is found to be weakly dependent on the secondary gun settings, somewhat different from ionic anorganic materials (Sec. III), but it still allows stable operation of the spectrometer. As could be expected, the spectra reveal that HREELS is very surface sensitive compared to ir and Raman spectroscopy for materials like polymers. Chain orientation at the polymer surface exposing terminal groups can be demonstrated,[10] which is less obvious in ir and Raman spectroscopy. The dependence of the HREELS cross section of polymers versus electron impact energy does not follow a $E^{-1/2}$ law like

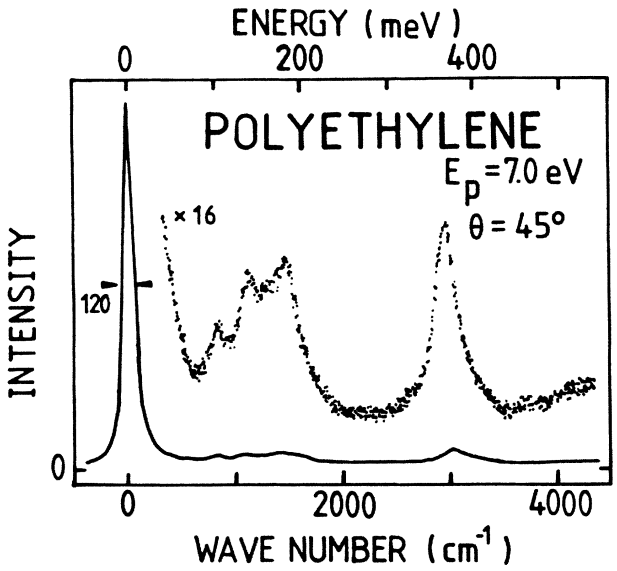

FIG. 4. Energy-loss spectrum of 7-eV electrons after reflection on a polyethylene surface. The losses are displayed on an extended scale.

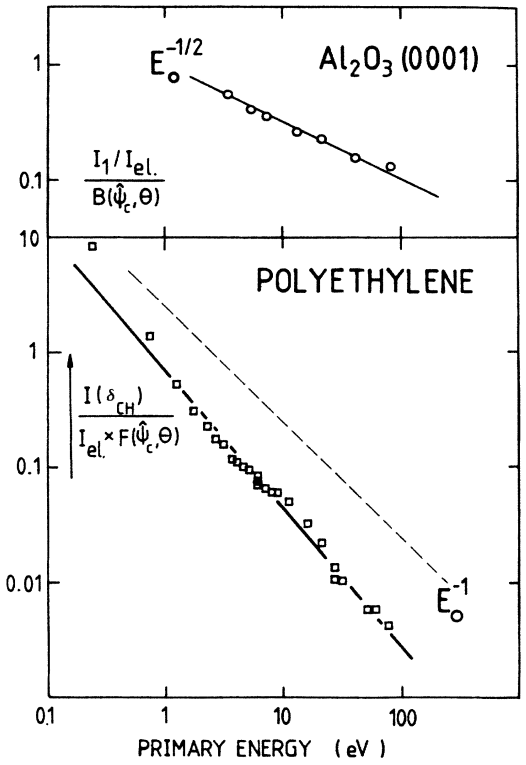

FIG. 5. Upper part: Excitation cross section for Fuchs-Kliewer phonons on Al_2O_3 following a $E_0^{-1/2}$ law, with E_0 the impact energy. The values are corrected for analyzer aperture effects $[B(\hat{\psi},\theta)]$ (Ref. 15). I_{el} is the elastic peak intensity, I_1 the first phonon loss intensity. Lower part: Excitation cross section of molecular vibrations in polyethylene versus impact energy E_0. The results are corrected for analyzer aperture effects $[F(\hat{\psi},\theta)]$. δ_{CH} represents the CH bending vibration. The results follow closely the E_0^{-1} dependence for isolated molecular vibrations.

for Fuchs-Kliewer phonons but a E^{-1} law characteristic of isolated molecular vibrations (Fig. 5). A polymer crystal behaves therefore more like a condensed gas rather than like a crystalline solid, not permitting long-range excitations or interactions.[17] This clearly demonstrates the potentialities of HREELS for this rather new field of surface science as well as the importance of the surface-potential stabilization technique.

II. THE SECONDARY ELECTRON BACKGROUND

A. General remarks

Irradiation of a sample with two kinds of electron beams creates a complex energy distribution of reflected electrons. The general shape of a spectrum spanning the whole range of energy is shown schematically in Fig. 6. One distinguishes two elastically reflected beams, one from the auxiliary high-energy gun and one from the HREELS monochromator.

Superimposed are backgrounds due to interband and Auger transitions as well as the "true" secondary background at very low kinetic energies reaching down to zero kinetic energy. The true secondary region represents the electron cascade distribution and band-structure-related peaks.[18] Interband and Auger transitions as well as nearly all of the secondaries background originate from the auxiliary gun.

A HREEL spectrum obtained in the range from the elastically reflected monochromatized beam down to the low-energy secondary-electron cutoff of a $Al_2O_3(1\bar{1}00)$ surface is shown in Fig. 7. It can be seen that the nearly linear background in the highly resolved spectra of the phonon losses in the energy range from 0 to 500 meV originates from the high-energy tail of the true secondary peak. For impact energies of 5 eV and more the intensity that is superimposed on the phonon spectra can be approximated by a straight line. Under optimal working conditions intensity ratios of the elastic peak to the se-

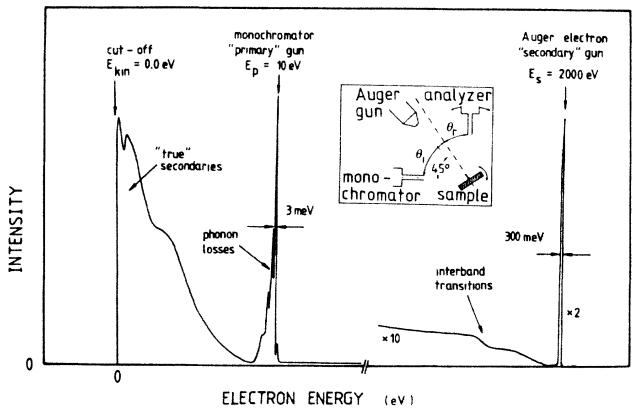

FIG. 6. Schematic energy distribution of reflected electrons delivered by an Auger electron gun and a HREEL spectrometer gun. The experimental geometry is shown schematically in an inset.

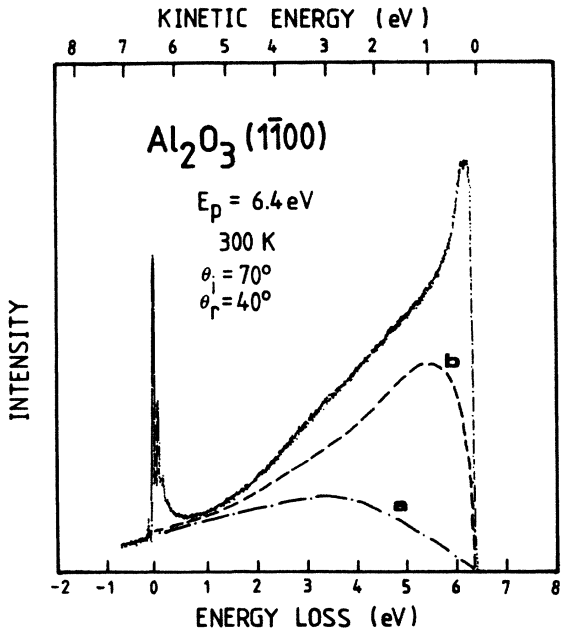

FIG. 7. Energy distribution of electrons reflected at or emitted from a $Al_2O_3(1\bar{1}00)$ sample. The distribution of the true secondaries has been attempted to fit with two different theoretical approaches (curve *a* and *b*) which are explained in the text.

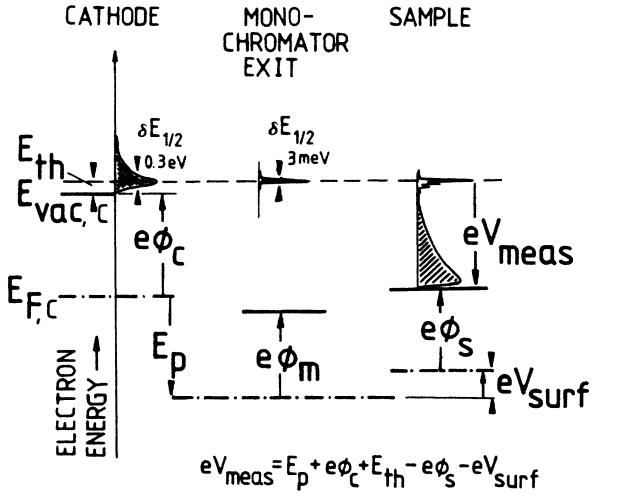

FIG. 8. Schematic energy-level diagram of the HREELS monochromator and the sample and the electron energy distributions occurring. The different symbols are explained in the text.

condaries background are in the range of 10^3 to 10^4. These high ratios are partially due to the different angular distributions of the reflected electrons: nearly isotropic for the secondary electrons (Sec. II B) and sharply centered around the specular direction for the phonon losses and the elastic peak.[5] The small analyzer aperture of about 1°—2° provides the selection of the interesting part of the spectrum for measurements in specular reflection, i.e., enhances the phonon losses over the secondaries. Quite high intensity ratios of up to 10^2 can, on the other hand, also be obtained on amorphous or rough samples, where the monochromatic beam after reflection on the sample is no longer well concentrated around the specular direction.

B. Work-function determination

The impact energy of the monochromatic beam can accurately be determined by measuring the energetic separation between the elastically reflected beam and the low-energy cutoff. Energy levels and distributions of electrons occurring through the HREEL spectrometer are shown schematically in Fig. 8. The electrons are emitted from a cathode filament at temperatures around 1300—1500 K. Their energy distribution therefore has a maximum at about 250—300 meV above the vacuum level (E_{th}); the distribution width being of the same order of magnitude. Cathode work function and Fermi level are indicated. The kinetic energy at the sample is obtained by applying an accelerating voltage between the target and the monochromator exit optics on one side and the filament on the other side (E_p). On the sample side, one distinguishes the sample work function ($e\phi_s$), the distance between the sample vacuum level and the elastically reflected beam (eV_{meas}), and a possible potential of the sample with respect to the surrounding optics (V_{surf}: deliberately applied or intrinsic charging). The distance between the sample vacuum level and the elastic peak can be measured by determining the energetic separation of the elastic peak and the cutoff of the secondary electrons.

This simple energy diagram allows us to cast the relation

$$eV_{\text{meas}}=E_p+e\phi_c+E_{th}-e\phi_s-eV_{\text{surf}}\ . \tag{1}$$

This equation is valid only when the sum $eV_{\text{surf}}+e\phi_s$ is larger than the monochromator exit work function $e\phi_m$; otherwise, electrons of very low energy are repelled towards the sample and the cutoff indicates only the monochromator work function. A correct measurement of $e\phi_s$ is obtained either through knowledge of the cathode work function and temperature or by measuring the work function of a reference material. Determinations via the cathode work function are not accurate because this necessitates precise knowledge of the filament work function and temperature, which are unknown for a not-well-cleaned tungsten filament, so that one is restricted to the determination of work-function changes or comparison to a reference. An accuracy of ±20 meV can be obtained on metal samples. An additional complication for insulators is a possible surface charge. Work functions can be derived under the assumption that only the charging state (eV_{surf}) and not the work-function ($e\phi_s$) changes for different currents and voltages of the auxiliary gun. The accuracy of this determination is somewhat limited (±50 meV).

An example of such a work-function determination is shown in Fig. 9 for $Al_2O_3(0001)$. Different voltages have been applied to the sample holder assuming that the sam-

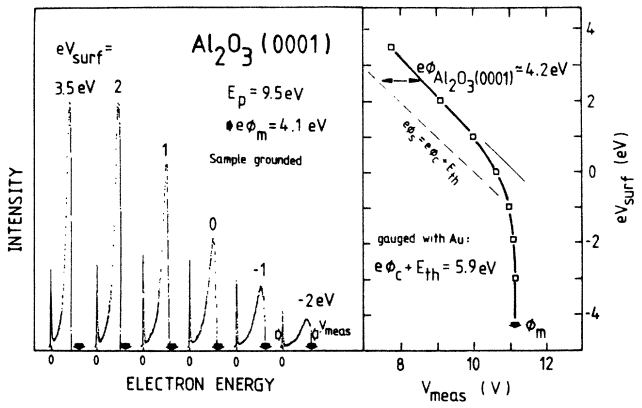

FIG. 9. Left-hand side: elastically reflected primary beam and secondary distribution for different voltages applied to a $Al_2O_3(0001)$ sample. The solid arrows indicate the cutoff due to the spectrometer optics; the open arrows indicate the meaning of the quantity V_{meas}. Right-hand side: plot of the measured quantity V_{meas} versus the applied potential. For negative voltages the work function can be derived from the distance towards the dashed-dotted line which has been obtained by a reference measurement with Au(110) ($\phi = 4.8$ eV).

ple surface potential follows these potentials within a narrow margin by means of a mechanism to be discussed in Sec. III. Clear changes in the secondary-electron distribution with respect to this voltage support the assumption. The measured quantity V_{meas} is indicated on the left-hand side of the figure and plotted against the applied voltage V_{surf} on the right-hand side. Only for strong negative voltages does the measured potential follow the expected straight line with a slope of -1. For positive voltages one determines the work function of the surrounding monochromator and analyzer optics (expt.: 4.1 eV). The sample work-function measurement has been gauged with a Au(110) (2×1) sample whose work function was taken from the literature to be 4.8 eV.[19] For the $Al_2O_3(0001)$ surface a work function of 4.2 eV can be derived from Fig. 9. The work function of MgO(100) was found to be 3.4 eV, the one for $Al_2O_3(1\bar{1}00)$ was 3.9 eV, and the one for polyethylene was 4.8 eV.

These work-function values are too high to represent the distance vacuum-level—conduction-band edge, which is, e.g., for Al_2O_3 on the order of 3.2 eV (Ref. 20) or less. The position of the Fermi level determined by these work-function measurements lies therefore in the forbidden gap of these insulators. One can raise the question about the meaningfulness of a Fermi-level definition in an insulator. Two explanations shall be tentatively offered.

For Al-oxide the work-function value found here agrees approximately with known Fermi-level positions when taking the Fermi-level—conduction-band distance found in tunnel junctions: 1.5 eV.[21] For the amorphous oxide in these junctions the Fermi-level position may be determined by defects like aluminum deficiencies.[22] In our single-crystalline samples a decomposition of the first layers with evaporation of oxygen creating Al clusters, or annihilation of color centers yielding the same effect also in the bulk, might be responsible for the creation of defect levels at the appropriate energy.

All work-function values obtained are quite independent of the auxiliary gun current; differences of less than 100 meV are found for intensity variations of more than 1 order of magnitude. One expects a change of the surface band bending for a changed nonequilibrium carrier density by, e.g., different trapping in surface states or by charge separation in a field due to band bending. This is, e.g., used to determine surface states in the gap of semiconductors with surface photovoltage spectroscopy.[23] Changes in the energetic separation of the Fermi level and the lower conduction-band edge of roughly 50—100 meV can, on the other hand, easily represent changes in the equilibrium carrier density of an order of magnitude. It will be shown (Sec. III) that the nonequilibrium carrier density follows nearly linearly the excitation current. One might therefore also tentatively assign the measured work functions as differences between sample vacuum level and an electron quasi-Fermi-level either in the forbidden gap or within a defect level. Quasi-Fermi-levels can be defined when the carrier distribution is a nonequilibrium distribution used to artificially describe the number of carriers in the respective band.[24] Either of the two above-mentioned explanations may apply for the Fermi level on an insulator under electron irradiation.

C. Secondary-electron energy distribution

The energetic distribution of secondary electrons has been calculated by a number of different authors; unfortunately, for reasons of complexity, calculations exist only for simple metals.[25] Willis performed angle-resolved secondary-electron emission measurements on graphite[26] and tungsten[27] and found well-structured distributions with maxima around 1 eV above the vacuum level for graphite and 10—20 eV for tungsten. This compares to the results for $Al_2O_3(1\bar{1}00)$ in Fig. 7. One sees a maximum very close to the sample vacuum level, resembling the graphite results, but the distribution is essentially structureless.

Model calculations of the energy distribution of secondary electrons based on a free-electron-gas model predict spectra of the general shape

$$N_{SEE}(E_{kin}) = 1/[A(E)(E_{kin}+E_0)^x] , \quad (2)$$

where E_{kin} is the electron kinetic energy, $A(E)$ is a geometric function, and E_0 is a theoretical parameter which is related to the position of the maximum of the distribution. The theory of Wolff,[28] which relates E_0 to the inner potential, gives maxima situated at rather elevated energies. Seah[18] pointed out, though, that the inner potential should be substituted by the Fermi level in Wolff's theory to better represent maxima at low energies found for Cu and Ag. An example of a distribution derived from Baroody[29] for a work function of 3 eV is shown as curve *a* in Fig. 7. This distribution gives similar results like Wolff's with the inner potential as a parameter for Li ($\phi = 2.4$ eV). The distribution has been normalized to the experimental curve for kinetic energies above 6 eV. A

somewhat better fit can be obtained by using a more recent theory of Chung[30] with the same value of 3 eV for the work function (curve *b*). Chung's theory uses Quinn's[31] expression for the mean free path and gets a maximum at roughly $\phi/3$ above the vacuum level. Both distributions clearly give too little intensity for kinetic energies close to the vacuum level. A further decrease of the parameter "work function" in Chung's theory gives too much intensity in the range 1–2 eV and too little at the sharp cusp.

No band-structure-related effects are expected for a material like a polymer which is not a well ordered, but only a pseudocrystalline, compound. Application of Chung's distributions for 3 and 2 eV work function are indicated (see Fig. 10, curves *a* and *b*, respectively). One sees a much closer agreement between theory and experimental distribution, especially for low angles of emission (closer to the sample normal). The cusp at very low kinetic energies has a quite marked angular dependence, being most intense at nearly grazing emission angle.

The most striking difference between the theoretical distributions and the experimental curves is the strong intensity of the experimental curves at low kinetic energies. To accommodate for this intensity one either has to assume extremely low work functions (following Chung's treatment) which are in no apparent relation to the work functions derived in the last paragraph, or to assume that the mean free path of the hot electrons has not been represented correctly. For Cu and Ag secondary emission has been found to be related to a free-electron level closely below the vacuum level.[18] Correspondingly, for ionic insulators the reference level may be the conduction-band edge instead of the Fermi level, which, of course, yields lower values for the theoretical parameter E_0. The second possible explanation for the deviation of the theoretical distributions from the experimental curves, the mean free path, seems also very probable, especially in view of the derivation of the mean free path which includes electron-hole pair creation as the most important limiting factor. This interaction should be completely absent in insulators for energies below the gap energy. In insulators, in general, one expects only longitudinal-optical-phonon excitation as scattering mechanisms,[32] at least for low electric fields.[33] The measured distribution contains furthermore a certain number of electrons, especially at low kinetic energies, which have suffered one or more collisions before leaving the sample (Sec. V). An additional effect which might also influence the secondary-electron distribution is the energy dependence of the secondaries production rate, which might be strongly influenced by band-structure effects and which is difficult to evaluate theoretically.[34]

The angular dependence of the sharp cusp close to the vacuum level, which is present for all insulating samples analyzed so far, is shown for $Al_2O_3(0001)$ in Fig. 11. As for polyethylene a marked intensity increase of this peak can be seen for large emission angles. This peak influ-

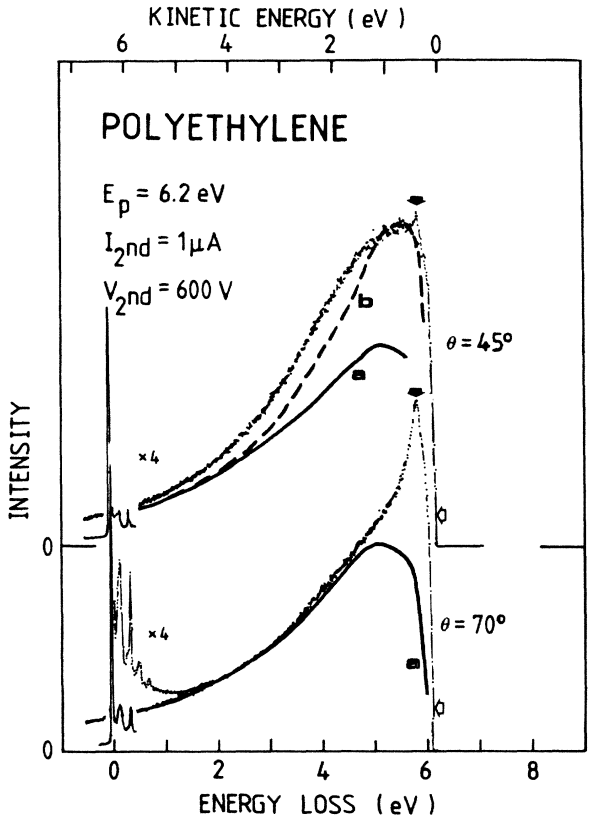

FIG. 10. Secondary-electron distributions of a polyethylene sample for different angles of emission (θ is measured from the surface normal). Fits have been done with the variable parameter (work function) being 3 eV (curves *a*) and 2 eV (curve *b*). The cusp at low kinetic energies is marked by solid arrows, the position of the cutoff by open arrows.

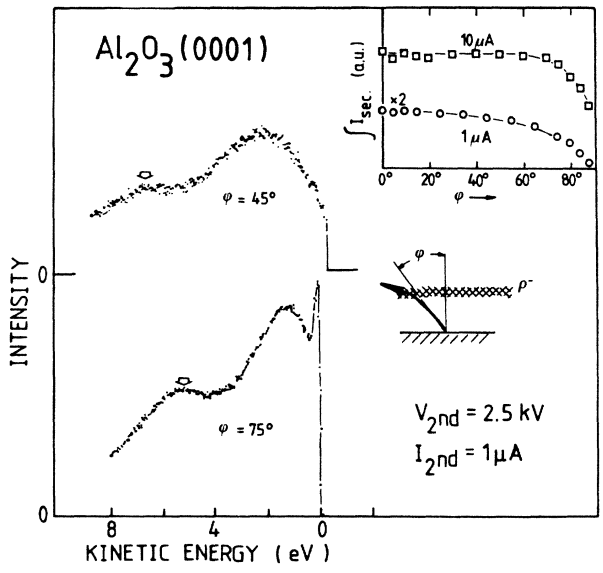

FIG. 11. Secondary-electron distribution of a $Al_2O_3(001)$ sample for two different angles of emission. The position of possible band-structure-related peaks is indicated. Inset: integrated intensity of the secondary-electron distribution for various angles of emission and for two different incident electron currents. Lower inset: the effect of a space-charge region on the trajectories of slow electrons is shown schematically.

ences the integrated intensity of the secondary electrons which should follow a $\cos\theta$ law. The integrated secondary-electron intensity is shown as an inset in Fig. 11 for two different gun currents. The distribution is found to be nearly constant for high currents, where this peak at low energies and high exit angles must then be dominant. Figure 9 shows a clear dependence of the energy distribution on the sample potential, the peak at low energies being most intense for high negative sample potentials. Any interpretation in terms of band-structure-related effects seems not probable because it can be seen for a wide variety of different insulators. This peak is interpreted as being related to a space-charge effect on the low-energy-electron trajectories. An electron cloud close to the sample surface will deviate the trajectories, especially those of the slow electrons towards higher exit angles, as indicated in Fig. 11. The small work-function difference between samples and spectrometer optics (4.1 eV) and the high secondary-electron yield of insulators favor the formation of a space-charge region. Its formation explains easily the electron gun current dependence of the cusp and the dependence on an applied negative voltage.

The unusually pronounced fine structure in the secondary emission of tungsten in comparison to other metals has been correlated to the existence of a gap in the band structure above the vacuum level.[27] This should increase the lifetime of hot electrons because the gap reduces the electron-hole pair scattering rate. From this point of view insulating samples should represent a still more promising class of materials because even electrons with moderate energy cannot excite electron-hole pairs at all. The only spectrum presented in this paper where a marked structure may be related to band-structure effects is $Al_2O_3(0001)$ in Fig. 11 (e.g., peaks denoted by open arrows). The vacuum level in Al_2O_3 is assumed to lie 3.2 eV above the lower conduction-band edge, and a variety of density-of-states maxima are found in the energy range from 1 to far above 3 eV beyond the vacuum level.[35] The position of the peaks in the experimental distribution is emission angle dependent, and such peaks occur as well on MgO and $Al_2O_3(1\bar{1}00)$ surfaces. We tentatively interpret these structures as being related to band-structure effects, e.g., maxima of the density of empty states. Any further interpretation, like an explanation of the absence of such structures for some emission angles, would require more extensive experiments.

III. NEUTRALIZATION MECHANISM

A. General remarks

The secondary-electron emission has been measured for a wide range of materials. It follows a universal yield curve.[25] Different materials generally exhibit different energies of maximum yield and a different maximal yield itself, which is usually largest for insulators due to fewer deexcitation possibilities for low-energy electrons. For an insulator surface under electron irradiation the secondary emission is less than one for energies below about 100 eV, rises to values as large as 20 for energies of several hundred eV to above 1 keV, and finally drops again below one

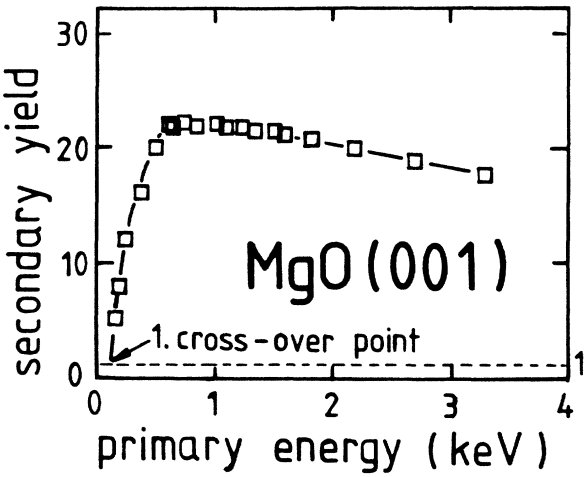

FIG. 12. Secondary-electron emission yield as a function of incident electron primary energy for MgO(001); after Ref. 36. Dashed curve: secondary yield equal to 1.

for kinetic energies of the order of several keV. This relationship, measured with a single-pulse beam retarding technique, is shown for a MgO single crystal[36] in Fig. 12. A low-energy electron beam with a total energy of several eV, as used in HREELS, will therefore charge an insulator surface negatively up to the beam energy. An electron beam with an energy exceeding the first crossover point, where the secondary yield becomes greater than unity, and below the second crossover point correspondingly tends to charge the sample positively by emission of secondary low-energy electrons. To compensate for a negative surface charge via secondary emission, a second electron beam with an energy between these two crossover points should be suitable.

A second mechanism that can be imagined to contribute to a surface-potential stabilization is the creation of a surface layer with an enhanced conductivity which allows surface charges to flow to ground potential. The creation of such a layer with an elevated number of nonequilibrium carriers is expected to take place under irradiation with high-energy electrons. The efficiency of this mechanism will depend on the mobility of the nonequilibrium carriers, on their lifetime, and on the lateral extent of the conducting layer. The questions to be answered experimentally are, (1) if such a compensation generates a stable or a metastable surface potential or, to put it another way, if the surface potential depends critically on the beam parameters of the higher-energy electron beam; (2) if both above-mentioned mechanisms contribute to the stabilization and to which extent; and (3) if they are both equally efficient in ensuring a stable potential.

B. Surface-potential measurement

The quantity derived from the energetic separation between the elastic peak and the secondary electron cutoff (Fig. 8) has been shown to be related to the sample surface potential by

$$eV_{\text{meas}} = E_p + e\phi_c + E_{th} - e\phi_s - eV_{\text{surf}} . \quad (3)$$

V_{surf} represents variations in the surface potential of the sample due to charging or work-function changes. The range of measurable charging is limited due to the surrounding spectrometer optics work function. As already mentioned, the distance between the elastic peak and the cutoff (V_{meas}) will reflect this quantity for positively charged samples. The accuracy and the limits of the measurement have been checked with an electrically isolated Au(110) sample in Fig. 13, where the charging, as determined with the spectrometer, is compared to the readings of a floating high impedance electrometer. Depending on the work function of the sample, the limiting measurable positive potential of a floating sample is about

$$V_{\text{surf}} = \phi_s - \phi_m - 0.2 \text{ V} , \quad (4)$$

$\phi_m = 4.1$ V. The potential of a sample with some conductance, either intrinsic or induced, can be measured accurately by applying a negative voltage to it. The precision of such a measurement is limited by the resolution of the spectrometer analyzer, which has been on the order of 10 meV for these measurements, and work-function fluctuations on the sample surface which will usually limit the actual precision attainable. The resolution can be judged from the steepness of the low-energy cutoff and the scatter in Fig. 13 (± 50 meV). Such measurements represent therefore a very sensitive probe for changes of the charging state of an insulating sample. It should be mentioned that a measurement of charging state of a sample does not require the use of the HREELS electron beam,[37] but its use clearly improves the accuracy.

The degree of positive charging of the Au sample in Fig. 13 is determined by the geometry of the experimental setup. An electric field will build up, depending on the potential of the sample surface and the distance towards a reference potential. The closer this reference potential (about 2 cm in the HREELS spectrometer) the less charging occurs, since the secondary electrons are more effectively repelled towards the sample.

Measurements of the energetic separation elastic peak—cutoff (V_{meas}) for several different voltages and currents of the high-energy electron gun are displayed in Fig. 14 for Al_2O_3 and polyethylene. For Al_2O_3 two different impact energies of the monochromatic beam have been used (4.5 and 9.5 eV, which are corrected for work-function differences in the figure) as well as different angles of incidence (45° and 70° for the monochromatic beam). Furthermore two different experimental configurations have been realized: once the sample holder was grounded during measurement, the other time it was floating. For the configuration with grounded sample holder, identical results were obtained with an additional negative voltage applied to the sample holder.

Looking first only at the Al_2O_3 results for a grounded sample holder, one sees that the surface potential is stable within 200 meV for a rather wide range of different secondary beam settings, energies, and angles of incidence. The strongest variations (about 200 meV) can be seen to occur for different angles of incidence, whereas in the range of energies from 300 to 5000 eV the surface poten-

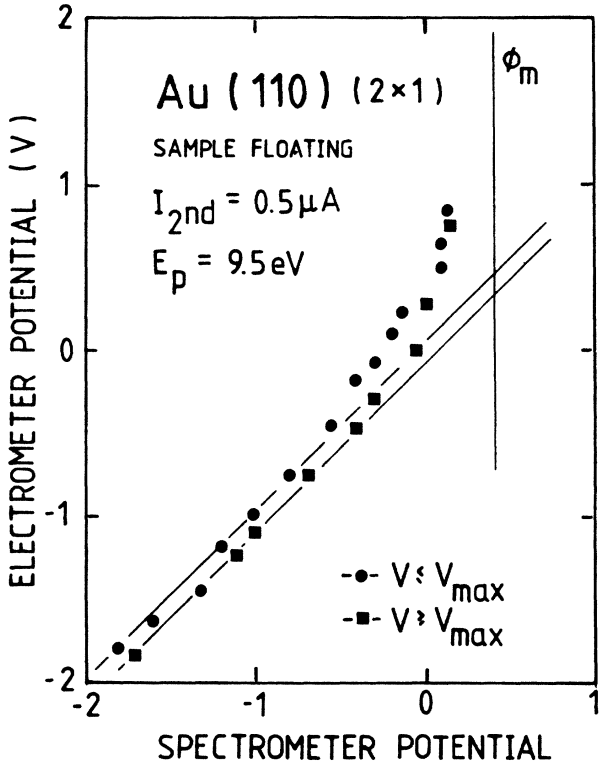

FIG. 13. Surface-potential measurement of a floating Au(110) (2×1) sample with an electrometer versus the HREEL spectrometer reading. The cutoff due to the spectrometer optics is indicated (ϕ_m). $V_{\max}$ is the voltage where maximum yield occurs.

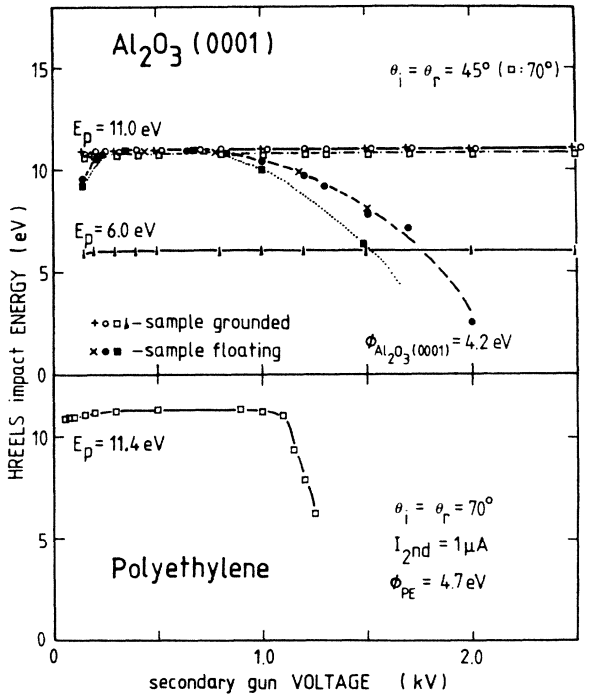

FIG. 14. Surface-potential measurements for $Al_2O_3(0001)$ and polyethylene for different parameters of the HREEL spectrometer. +, 0.1 μA; ○, 10 μA secondary current at $E_p = 11$ eV and $\theta = 45°$; □, 1 μA at $E_p = 11$ eV and 70°; △, $E_p = 6$ eV and $\theta = 45°$, 1 μA (all for a grounded sample). ■, 0.2 μA; ●, 1 μA; ×, 10 μA for 45° and $E_p = 11$ eV (all for a floating sample).

tial stays within 50 meV for a given angle of incidence. Stronger deviations (up to 200 meV) can be seen for energies down to 150 eV.

We conclude from this measurement that the technique presented in this paper provides a very stable surface potential on ionic insulators, i.e., almost a surface neutralization. The same stability can be seen for the polyethylene sample in a more restricted range of energies of the secondary beam (300 to 1000 eV). The presented method is therefore a reliable tool for creating stable surface potentials on a wide range of insulating materials.

C. Potential stabilization by induced conductivity

In the configuration where the sample holder is grounded a number of currents enter and/or leave the sample under irradiation (Fig. 15). Here we have the low-energy monochromatic beam that does create nearly no secondaries and its reflected part, the high-energy electron beam with its reflected part and the corresponding low-energy secondary electrons, and finally the current that passes from or towards ground potential via some sample conductivity, which is either intrinsic or radiation induced. One may neglect, in a first approximation, the influence of the monochromatic low-energy current on the secondary-electron emission. This is justified by the measurements displayed in the lower part of Fig. 16, where the secondary-electron distribution is shown once with the HREELS beam probing the sample surface and once without it. No differences in the distributions can be seen. The monochromatic low-energy beam is not compensated by additional emission of low-energy secondary electrons.

The remaining currents suitable for charge compensation are the reflected part of the high-energy beam and the sample conductivity towards ground potential (Fig. 15). The surface-potential stabilization only works this way if the whole sample surface is irradiated by the high-energy beam (completely defocused beam). Under these conditions the irradiated area reaches the tungsten clamps with which the sample is kept in place and which are at a reference potential. We can thus exclude the reflected part of the high-energy beam as a possible source of the stabilization, also because surface-potential changes of less than 200 meV should not influence a beam with energy of several keV, e.g., via a changed reflectivity.

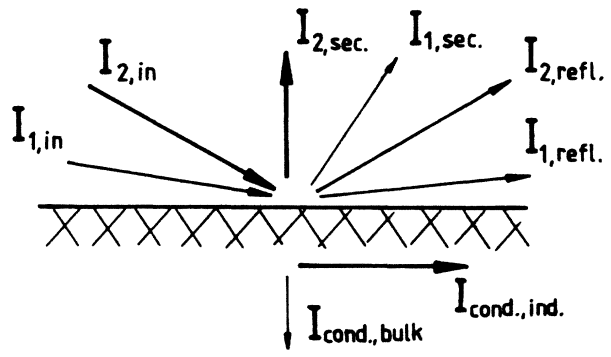

FIG. 15. Electron currents entering and leaving the sample. Primary gun in $I_{1,\mathrm{in}}$, reflected part out, $I_{1,\mathrm{refl}}$; the same for the secondary gun, $I_{2,\mathrm{in}}$, $I_{2,\mathrm{refl}}$; true secondary currents out, $I_{1,\mathrm{sec}}$ and $I_{2,\mathrm{sec}}$; and currents due to conductivity in the bulk $I_{\mathrm{cond,bulk}}$ and induced at the surface $I_{\mathrm{cond,ind}}$.

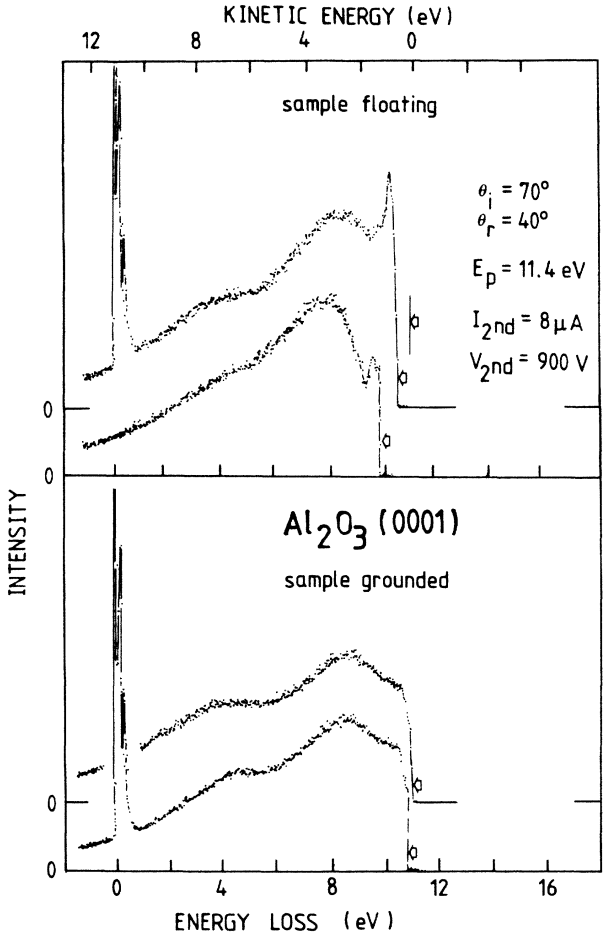

FIG. 16. Secondary-electron distribution of $Al_2O_3(0001)$ with and without primary beam reflected at the surface. Upper part: sample floating; lower part: sample grounded. The cutoff to be expected for the spectrometer optics as well as the measured cutoffs are indicated by open arrows.

An induced surface conductivity as the origin of potential stabilization explains the stability, starting from an energy where enough secondary electrons in the sample are created to provide sufficient conductivity (close to the first crossover point). For high energies the conducting layer will be more in the bulk of the sample due to the high penetration depth of the electrons creating secondaries further away from the surface. The potential stabilization by induced sample conductivity is thus independent on the secondary emission, but still related to the secondary creation rate. The strongest support for the conductivity influence are the drastic changes of sample potential and secondary-electron emission that occur when the sample-surface—ground-potential current is suppressed by keeping the sample floating (Fig. 16). An enhanced surface conductivity requires a certain free-

carrier density. A rough estimation with Ohm's law based on the sample area (1 cm^2), the maximal incident current (10^{-5} A), and surface potential (100 mV) yields a sample resistivity of 0.01 up to 10 Ω cm, depending on the thickness of the conducting layer (assuming a range from 10 nm to 10 μm). With existing literature data of the carrier mobility[38] one expects carrier densities of 10^{20} cm^{-3} or less. Such densities are known to have marked effects on the vibrational HREEL spectra, e.g., via Landau damping, Drude damping, or plasmon creation in the free-carrier gas. A numerical evaluation to give order-of-magnitude estimation of these effects will be given in Sec. IV.

D. Potential stabilization by enhanced secondary-electron emission

The remaining mechanism, induced conductivity excluded by keeping the sample floating, is obviously less efficient (Fig. 14). Charging effects of several volts occur in the low-energy range below about 200 eV and in the range about 800—1000 eV. In the intermediate range, where the secondary-electron emission of the sample is strongest, the potential seems to be almost as stable as with the sample-ground current present. One has to keep in mind, though, that the presented technique is insensitive towards positive sample charging when the sample is floating.

The high-energy electron beam generates a cloud of very-low-energy secondary electrons close to the sample surface. Figure 7 shows that most of these electrons have energies on the order of about 1 eV and below, followed by a tail extending to about 10—20 eV. Part of these electrons can be used to keep the surface potential constant. Under illumination with electrons that have a secondary yield greater than one a sample that is not grounded will tend to charge up since it cannot deliver the required current via some bulk conductivity. This charging will reach a saturation value which keeps back as many secondary electrons as necessary to ensure a zero net current. Depending on the experimental geometry, an electric field builds up that reflects low-energy electrons back to the sample surface. As found for Au(110), only rather small positive voltages are obtained due to the small sample-spectrometer optics distances. One does not expect much stronger charging for insulators despite the high yield due to the lower average kinetic energy of the secondaries. Close to the crossover points too little secondary electrons are emitted to keep the sample potential constant; it starts to charge negatively. For primary energies far from the crossover points two cases are to be distinguished. Electrons with energies below the first crossover point will tend to charge the sample up to the primary energy to completely reflect any incoming electron. For electrons above the second crossover point the sample will charge up to the point where the electrons are sufficiently decelerated to enter the region of high secondary yield.

Considering conditions close to the maximum yield, this surface-potential stabilization mechanism should also be able to accommodate for a supplementary smaller current of either polarity like the one delivered by the HREEL spectrometer. Figure 16 shows the secondary-electron distribution for a floating Al_2O_3 sample once with and once without the monochromatic electron beam. One distinguishes, besides a rather smooth and broad background, a sharp maximum in the secondary distribution close to the cutoff when the monochromatic beam is on. The part of the monochromatic beam that enters the sample is therefore balanced by additional secondary electrons emitted close to the cutoff, i.e., those with the lowest kinetic energies. A change of the surface potential accompanies these additional electron currents because the general shape of the secondaries distribution is not changed. The surface potential in this configuration is obviously stabilized by enhanced secondary-electron emission. The effectiveness of this mechanism is restricted to electron energies close to the maximum of the secondary yield curve, causing the narrower range of stable potential seen in Fig. 14. For too low secondary currents the primary beam no longer interacts completely with the sample so that the absorbed quantity of electrons, which has to be balanced, decreases.

The region of stable surface potential for polymer samples reflects their smaller secondary yield compared to that of ionic insulators.[39] The second crossover point is consequently lower, on the order of 800—1500 eV. As could be expected, the region of stable surface potential is narrower and exhibits charging effects for energies above 1200 eV.

IV. AUXILIARY GUN INFLUENCES ON VIBRATIONAL SPECTRA

A. Phonon excitation cross section

Changes of the two free parameters of the auxiliary electron gun, its voltage and current, have several influences on the recorded HREEL spectra of Fuchs-Kliewer phonons. The secondaries can influence the resolution of the spectra, their intensity, or the excitation probability of the phonons. Whereas a good resolution and a high intensity of the spectra are desirable features, the excitation probability of the phonons is a physical quantity that has to be absolutely independent of the auxiliary gun parameters to make the method useful at all.

The intensity of Fuchs-Kliewer phonons and their multiples, as seen in Fig. 2, follows a Poisson distribution[16] at low temperature. The excitation probability is obtained from the experiment by numerical calculation of the single-phonon loss function, which is self-convoluted to reproduce the Poisson distribution, convoluted with the instrument transfer function, and the result is fitted to the experimental spectra.[7,8] The excitation probability is a function of the scattering angle and of the impact energy and allows us to calculate the charge transfer between the ionic sublattices close to the surface.

The excitation probability for a 70° angle of incidence and an 11.0 eV impact energy is shown in Fig. 17 for different voltages of the secondary-electron gun on an $Al_2O_3(0001)$ sample. Two different excitation probabilities are plotted: the ratio of the elastic peak to the first phonon loss I_0/I_1 and the ratio of the first loss to the second loss I_1/I_2. It is important to note that higher ex-

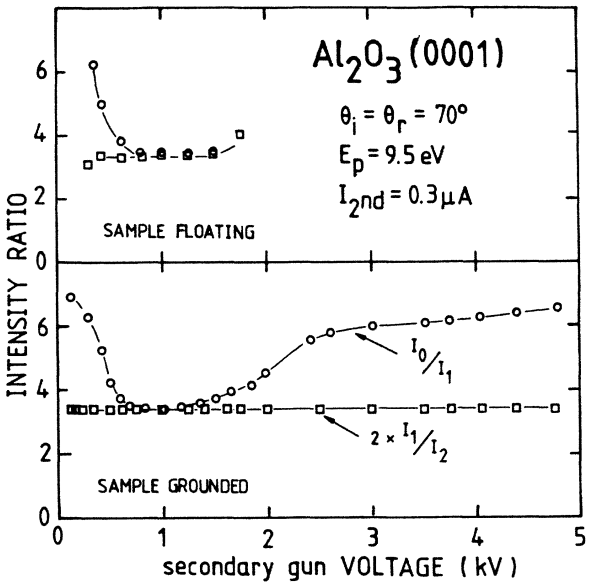

FIG. 17. Inverse phonon excitation cross section of Fuchs-Kliewer phonons on $Al_2O_3(0001)$ for different secondary gun voltages in two different experimental configurations; sample grounded and floating. Shown are the ratios of elastic beam to first phonon loss intensity I_0/I_1 and the ratio of the first loss to second loss intensity I_1/I_2, corrected to fit the Poisson distribution (times 2).

citations like I_2 originate from multiple scattering and not from anharmonic contributions. Whereas the ratio I_1/I_2 is constant in the whole range of voltages, the ratio I_0/I_1 rises above this value for voltages below about 0.7 keV and above about 1.5 keV electron energy. It seems that part of the elastic beam does not interact fully with the sample below and above some critical electron energy, but that all electrons that do interact with the sample exhibit a constant excitation cross section. We conclude from these results that for secondary gun energies between 0.7 and 1.5 keV, stable and reproducible results can be obtained that allow reliable deduction of materials parameters. Even beyond these limits reasonable results can be obtained, keeping in mind that part of the incident electron beam does not interact with the sample. Essentially the same results, with somewhat larger error bars, are found for a floating sample. Below about 0.8 keV and above 1.6 keV electron energy the surface potential may not be completely stable along the entire surface, reflecting part of the monochromatic low-energy beam before any interaction with the substrate has taken place. This can be imagined as incomplete potential stabilization yielding a patchy surface potential. The most reliable results can therefore be obtained when both above-mentioned stabilization mechanisms are efficient, i.e., grounded samples with secondary gun voltages close to the maximum secondary yield. For polymer samples the range of parameters of the second electron gun is mainly determined by the energy range in which the secondary emission is greater than unity.

B. Nonequilibrium carrier conduction

The resolution of HREEL spectra is influenced by the auxiliary gun current as shown in the lower part of Fig. 18 for MgO(001). The full width at half maximum (FWHM) of the elastic peak increases for very low currents for the same reason as for too low or too high gun voltages: a nonconstant surface potential. At high currents, the resolution slowly degrades again. The shape of the elastic peak changes for an increased secondary gun current. As shown in the upper part of the figure, the peak at high currents can be obtained from that at low currents (best resolution obtainable) by convolution with a Lorentzian of the indicated FWHM. Convolutions with a Gaussian gave less good agreement with the experiment. These results allow some order of magnitude estimations about the nonequilibrium carriers in MgO.

Two mechanisms may be responsible for the broadening of the elastic peak: Drude damping, which implies a finite lifetime of the carriers by an electron-electron scattering mechanism, or low-energy plasmon creation.[40] By assuming that the broadening is entirely due to either one of these mechanisms, one can derive order-of-magnitude estimations for nonequilibrium carrier densities, lifetimes, and mobilities. Since it will be shown that both mechanism contribute, this approach seems justified.

If we suppose the broadening were caused by low-energy plasmons, an upper limit of the carrier density can be calculated. For the dependence of the carrier density on the plasmon frequency one finds

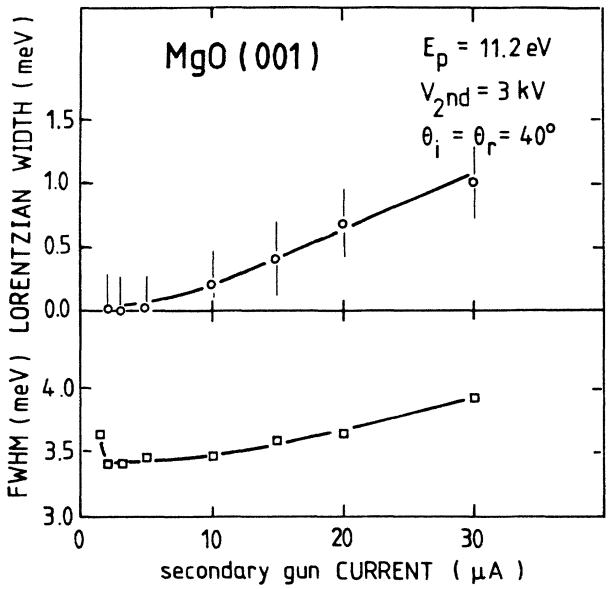

FIG. 18. Full width at half maximum (FWHM) of the elastic peak on a MgO(001) sample for different secondary gun currents. Upper part: elastic peak from which the resolution in the lower part was obtained, fitted by a convolution of the elastic peak at 2 μA secondary gun current and a Lorentzian of the given full width.

$$n=\frac{\epsilon_0 m^* \omega_p^2}{e^2}\ , \tag{5}$$

where ϵ_0 is the vacuum permittivity, m^* the effective mass of the conduction electrons, ω_p the plasmon frequency, and e the electron charge. 0.3 meV is assumed to be the upper plasmon energy (Fig. 18). The effective mass of electrons close to the bottom of the conduction band at the Γ point in MgO is about one free-electron mass. Light holes with $0.1m_e$ and $1m_e$ exist also.[41] Inserting these values in (5) yields an upper limit of the carrier density of about 10^{13} to 10^{14} cm^{-3}. To obtain the same order of magnitude with the simple estimation of Sec. III, using Ohm's law, one has to assume a layer thickness of about 10 μm, where nonequilibrium carriers exist, sample resistivities of about 10 Ω cm, and carrier mobilities of 10^4 cm^2/V sec, which are much higher than previously published data.[38] For the following we accept these results and check them for self-consistency.

Persson and Demuth[40] derived an expression that permitted us to distinguish between Drude damping and plasmon creation for thin conducting overlayers. A parameter $\hbar\beta$ has to be larger than kT (k is the Boltzmann constant, T is the temperature) for Drude damping and smaller than kT for plasmon creation to be the main mechanism causing peak broadening. The parameter is expressed by

$$\hbar\beta=\frac{mn^*e^2}{m^*\epsilon_0(\epsilon+1)k}\ , \tag{6}$$

where n^* is the carrier density per unit area, ϵ the sample dielectric constant [$\epsilon_\infty=3$ for MgO (Ref. 42)], and k the wave vector of the incident electron ($E_p=10$ eV). A value on the order of 10 meV is obtained for $\hbar\beta$. Since this is on the order of kT (25 meV) both mechanisms have to be considered to contribute to the peak broadening. The change of the peak shape, on the other hand, permits us to decide which is the more important one. For a peak broadening due to plasmon creation one expects a change towards a Gaussian, for Drude damping towards more Lorentzian shape.[40] The main peak-broadening mechanism is thus Drude damping.

An expression derived by the same authors[40] for Drude damping permits us to estimate a scattering time τ, the inverse Drude damping. They derive for the half-width the expression

$$\Gamma=\frac{8kTh(\alpha,\xi)}{\pi\cos^2\alpha k a_0}\frac{1}{\epsilon+1}\ , \tag{7}$$

where the half-width Γ is in meV, α is the measurement angle (60°), a_0 is the Bohr radius, and $h(\alpha,\xi)$ is a function related to $\beta\tau$ which is plotted in Ref. 40. Since the value of $h(\alpha,\xi)$ obtained is rather small, a linear approximation has been assumed between $h(\alpha,\xi)$ and $(\beta\tau)^{-1}$. The value for $\beta\tau$ obtained with the above parameters is $\beta\tau=40$. Together with the value for $\beta=10$ meV/$\hbar$ a scattering time of about 5×10^{-12} sec is obtained. This time is comparatively long: in semiconductors, scattering times are usually of the order of 10^{-13} sec; in metals, about 10^{-14} sec. On the other hand, the scattering mechanism in insulators is distinctly different from other materials, excluding electron-hole pair creation and allowing only optical-phonon scattering.[32] A time of several 10^{-12} sec seems not unphysically long. With simple free-electron relations further quantities can be derived. The resistivity

$$\rho=\frac{m^*}{ne^2\tau} \tag{8}$$

is found to be about 1 Ω cm in agreement with results above.

The mobility

$$\mu=\frac{e\tau}{m^*} \tag{9}$$

is on the order of 10^4 to 10^5 cm^2/V sec, again on the same order of magnitude as the above results. The results obtained are self-consistent in that they all point to the same order of magnitude of resistivity and carrier density. The high mobility, which is caused by the long scattering time, results in a long mean free path of roughly 1 μm or less. There are only very few experimental or theoretical results for mean free paths of electrons (or holes) of energies of a few eV above the conduction-band edge (Fermi level for metals). For potassium[43] values up to 0.1 μm are expected for electrons of 2 eV above the Fermi level. Due to the absence of electron-hole pair creation one expects the mean-free-path values in insulators to be longer.[44] The only mean-free-path values in insulators known to us are those derived from tunneling or carrier injection experiments, which all use either Al-oxide, GaAs, or silicon dioxide. For energies of about 1 eV above the conduction-band edge of Al-oxide, mean free paths of about 20 nm were found;[45] larger values up to 1 μm should occur for lower energies. The structure of the barrier materials used is quite different; tunnel barriers are amorphous instead of single crystalline. One expects again the mean free path to be longer in single-crystalline MgO due to the absence of defect scattering. A mean free path of about 1 μm signifies that most of the excited carriers are within a range quite close to the conduction-band edge, say within several 100 meV.[46] The nonequilibrium carrier generation rate in a material like MgO must be above 10^{16} cm^{-2}sec^{-1} for incident currents of 10^{-5} A. A steady-state carrier density of 10^{11} cm^{-2} implies recombination rates of 10^5 sec^{-1} or more, which implies average lifetimes $\hat{\tau}$ until recombination of less than 10^{-5} sec. For such lifetimes a drift velocity

$$v_{\text{drift}}=\frac{eE\hat{\tau}}{2m^*} \tag{10}$$

can be calculated. With electric fields of 10 V/m drift velocities of 10 m/sec are obtained. Such velocities are in agreement with an extrapolation from limiting drift velocities of 10^4 m/sec in Si and Ge reached at 10^5 V/m.[47] A drift velocity of 10 m/sec or less gives drift lengths of less than 100 μm. This correlates to the assumption of a layer of 10 μm where nonequilibrium carriers are present, as derived from resistivity considerations. Such drift lengths explain the experimental finding that complete illumination of the insulating sample is necessary to install the induced current potential stabilization mechanism.

The low carrier density necessary in insulators has a further consequence for the HREEL spectra. Landau damping of collective excitations like plasmons or phonons occur when electron-hole pair excitations with the same energy and momentum are possible.[48]

Landau damping can be detected with HREELS because quite large momentum transfers can be measured for low-energy electrons. These effects do not occur in insulators since the low Fermi momentum

$$k_F=(3\pi^2 n)^{1/3} \tag{11}$$

of less than 3×10^{-3} Å^{-1} places the range where Landau damping occurs at least 2 orders of magnitude out of the range of momentum transfers measurable with usual impact energies.

V. RADIATION DAMAGE DUE TO ELECTRON IRRADIATION

A. Ionic insulators

Irradiation with high-energy electrons is known to create defects in ionic insulators as well as in polymers. For the applicability of the proposed potential stabilization technique, only the possible influences of these defects on the vibrational loss spectra are concerned. The nature of the defects is very different for the two classes of materials.

Electron injection into ionic insulators creates color centers. This can be seen optically after prolonged irradiation of the samples with high current densities. Both Al_2O_3 and MgO show a brownish color where the irradiation was strongest. These color centers yield characteristic energy losses in the HREEL spectra at loss energies of several eV.[49] The time and current densities necessary for perceptible color center creation are rather elevated: 10^{-6} A/cm^{-2} at 2 keV for several hours. The presence of color centers influences the HREEL vibrational spectra only indirectly. Due to the large spatial extent of the Fuchs-Kliewer phonons their excitation cross section, half-width, and energetic position is not changed by the presence of color centers close to the sample surface. The irradiation may, on the other hand, lead to creation of vibrations localized at these lattice irregularities. The presence of color centers does change the reflectivity of the sample, either via the charges trapped in them or by their influence on recombination cross sections and rates for the nonequilibrium carriers. An irreversible change in the sample reflectivity can be seen to occur on an oxide sample after prolonged irradiation (Fig. 19). All these changes can be reversed by thermal anneal of the sample to rather moderate temperatures (900 K) in air or *in vacuo,* because the color centers are annihilated at these temperatures via migration towards the surface.

B. Polymers

In polymer samples, surface decomposition of the compound occurs under irradiation with fast electrons.[50] The decomposition can first be seen in the displacement of the high-energy secondary emission crossover point. An almost exponential decrease of the high-energy threshold can be observed even for moderate irradiation current densities and in rather short times (Fig. 20). The quantity of defects created seems to be rather small because even after prolonged measurements the vibrational spectra do not exhibit additional features or changes in the peak intensity ratios. Their number has to be on the order of $\frac{1}{10}$ to $\frac{1}{100}$ of the number of molecules probed by the monochromatic electron beam, i.e., 10^{13} cm^{-2} in a probed depth of about ten monolayers. The presence of supplementary vibrations is difficult to verify for polymers due to the rather limited resolution of the spectra (Fig. 4). Any changes occurring on the polymer surface are of course irreversible, and the measurement time and current

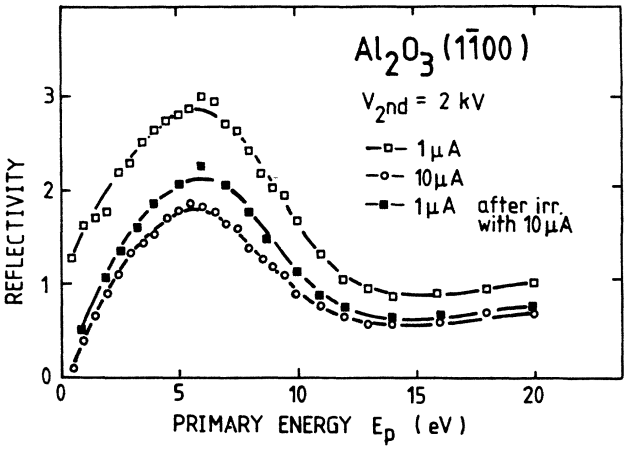

FIG. 19. Reflectivity of a $Al_2O_3(1\bar{1}00)$ sample for the primary beam versus beam energy for different currents of the secondary gun: □, 1 μA; ○, 10 μA; and ■, 1 μA after prolonged irradiation with 10 μA. The reflectivity changes due to defect creation.

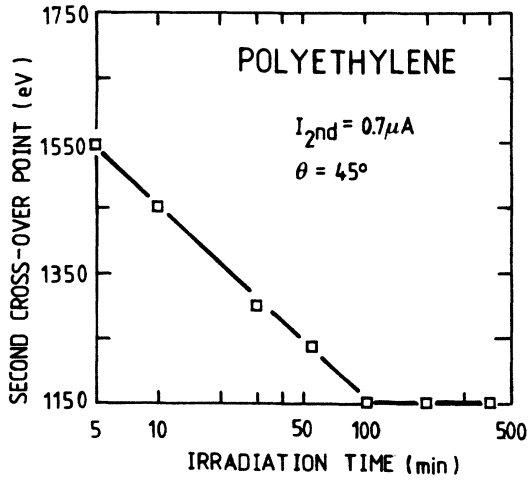

FIG. 20. Second crossover point (secondary yield passes through 1) as a function of irradiation time for polyethylene. The yield diminishes due to defect creation.

density therefore have to be restricted to a minimum.

The irradiation with high-energy electron does influence the secondary-electron distribution (Fig. 21). Prolonged irradiation displaces the maximum of the distribution towards lower energies and reduces the overall intensity. This is tentatively explained by shorter mean free paths after irradiation, causing a faster thermalization of the nonequilibrium carriers. A shorter mean free path requires additional scattering centers like structural defects. The assumption that the secondary-electron distribution is formed only by electrons having suffered no collisions[29] after creation is therefore not justified[46] at least for polymers.

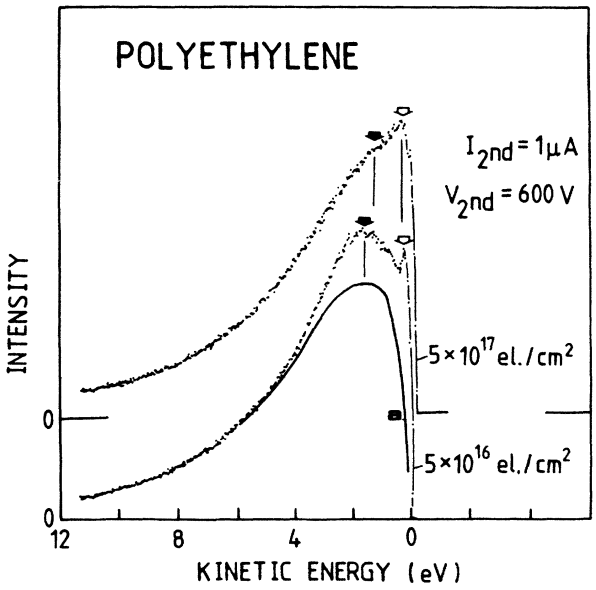

FIG. 21. Secondary-electron distribution of polyethylene after two different irradiation dosages. The maximum of the distribution (solid arrows) shifts towards lower kinetic energies due to defect creation. Curve *a* represents a fit with Chung's theory for a work function of 4 eV. The low-energy cusp does not change position (open arrows).

CONCLUSIONS

An experimental method has been described that allows us to take HREEL vibrational spectra of excellent quality on insulating samples of very different kinds, like ionic insulators or polymers. The method consists in irradiating the sample surface with the defocused beam of an auxiliary electron gun working in the ranges of voltage and current of a typical Auger electron spectrometer gun, thus making the method easily adaptable to every HREEL spectrometer. The method permits us to take spectra which allow quantitative comparison with theoretical calculations and, in the case of ionic insulators, perfect agreement with the theory has been found. The mechanism of surface-potential stabilization has been found to depend somewhat on the sample material, i.e., on its secondary-electron emission coefficient and its hot carrier conduction mechanism. Surface-potential stabilization is obtained either by creation of a conducting layer close to the sample surface which permits accumulated charges to flow to ground potential or, somewhat less efficient, by enhanced emission of secondary electrons close to the sample vacuum level. Both mechanisms are present in the general case but contribute differently, depending on the sample material and/or the experimental arrangement. A range of optimal parameters to obtain HREEL vibrational spectra has been given and any deterioration of the spectra has been correlated to patchy surface potentials. Drude damping and/or surface-plasmon creation in the nonequilibrium free-carrier gas has been found and estimations of carrier densities, lifetime, and mean free path were given. Landau damping has been found not to contribute in insulators within the given experimental conditions. Negative influences of the irradiation of the insulators with high-energy electrons like color center creation or sample surface decomposition have been found to be very limited with respect to the vibrational spectra. The method is therefore thought to be a valuable tool to complete the range of materials which can be studied by electron-energy-loss spectroscopy.

ACKNOWLEDGMENTS

This work is supported by the Belgian Fund for Joint Basic Research and by the Belgian Ministry for Science Policy [Institut de Recherche sur les Interfaces Solides (IRIS) project]. One of us (J.J.P.) is supported by the Belgium National Fund for Scientific Research.

*Present address: IBM Thomas J. Watson Research Center, Yorktown Heights, NY 10598.

[1]H. W. Werner and N. Warmoltz, J. Vac. Sci. Technol. A 2, 726 (1984).

[2]G. Slodzian, Ann. Phys. (Paris) 9, 591 (1964).

[3]I. A. Abroyan, V. P. Lavrov, and I. G. Fedorova, Fiz. Tverd. Tela (Leningrad) 7, 3660 (1965) [Sov. Phys.—Solid State 7, 2954 (1966)].

[4]H. Onuki, H. Iwamoto, and R. Onaka, Solid State Commun. 34, 941 (1980).

[5]H. Ibach and D. L. Mills, *Electron Energy Loss Spectroscopy and Surface Vibrations* (Academic, New York, 1982).

[6]*Vibrational Spectroscopy of Adsorbates,* edited by R. F. Willis (Springer, Berlin, 1980).

[7]M. Liehr, P. A. Thiry, J. J. Pireaux, and R. Caudano, J. Vac. Sci. Technol. A 2, 1079 (1984).

[8]P. A. Thiry, M. Liehr, J. J. Pireaux, and R. Caudano, Phys. Rev. B 29, 4824 (1984).

[9]Ph. Lambin, J. P. Vigneron, and A. A. Lucas, Phys. Rev. B **32**, 8203 (1985).
[10]J. J. Pireaux, P. A. Thiry, R. Caudano, and P. Pfluger, J. Chem. Phys. (to be published).
[11]J. J. Pireaux, P. A. Thiry, and R. Caudano, Surf. Sci. **162**, 132 (1985).
[12]H. Ibach, Phys. Rev. Lett. **24**, 1416 (1970).
[13]A. A. Lucas and M. Sunjic, Prog. Surf. Sci. **2**, Pt. 2, 75 (1972).
[14]A. A. Lucas and J. P. Vigneron, Solid State Commun. **49**, 327 (1984).
[15]E. Evans and D. L. Mills, Phys. Rev. B **5**, 4126 (1972).
[16]P. A. Thiry, M. Liehr, J. J. Pireaux, R. Sporken, R. Caudano, J. P. Vigneron, and A. A. Lucas, J. Vac. Sci. Technol. B **3**, 1118 (1985).
[17]N. Ueno, W. Gadeke, E. E. Koch, R. Engelhardt, and R. Dudde, J. Electron Spectrosc. Relat. Phenom. **36**, 143 (1985).
[18]M. P. Seah, Surf. Sci. **17**, 132 (1969).
[19]P. Vernier, E. Croquet, and M. Bigueure, C. R. Acad. Sci. **262**, 1728 (1966).
[20]V. A. Fomichev, Fiz. Tverd. Tela (Leningrad) **8**, 2892 (1966) [Sov. Phys.—Solid State **8**, 2312 (1967)].
[21]K. H. Gundlach and G. Heldmann, Phys. Status Solidi **21**, 575 (1967).
[22]K. Wefers and G. M. Bell, Technical paper No. 19, ALCOA Research Laboratory, 1972 (unpublished).
[23]H. C. Gatos and J. Lagowski, J. Vac. Sci. Technol. **10**, 130 (1973).
[24]W. Shockley, Bell Syst. Techn. J. **28**, 435 (1949).
[25]A. J. Dekker, in *Solid State Physics,* edited by F. Seitz and D. Turnbull (Academic, New York, 1958), Vol. 6.
[26]R. F. Willis, B. Feuerbacher, and B. Fitton, Phys. Rev. B **4**, 2441 (1971).
[27]R. F. Willis and N. E. Christensen, Phys. Rev. B **18**, 5140 (1978).
[28]P. A. Wolff, Phys. Rev. **95**, 56 (1954).
[29]E. M. Baroody, Phys. Rev. **78**, 780 (1950).
[30]M. S. Chung and T. E. Everhart, J. Appl. Phys. **45**, 707 (1974).
[31]J. J. Quinn, Phys. Rev. **126**, 1453 (1962).
[32]K. K. Thornber and R. P. Feynman, Phys. Rev. B **1**, 4099 (1970).
[33]T. N. Theis, D. J. DiMaria, J. R. Kirtley, and D. W. Dong, Phys. Rev. Lett. **52**, 1445 (1984).
[34]A. Van der Ziel, Phys. Rev. **92**, 35 (1953).
[35]I. P. Batra, J. Phys. C **15**, 5399 (1982).
[36]N. R. Whetten and A. B. Laponsky, J. Appl. Phys. **30**, 432 (1959).
[37]J. P. Vigouroux, J. P. Duraud, A. LeMoel, C. LeGressus, and C. Boizian, Nucl. Instrum. Methods Phys. Res. B **1**, 521 (1984).
[38]J. H. Pollard, D. L. Bowler, and M. A. Pomerantz, J. Phys. Chem. Solids **26**, 1325 (1965).
[39]R. F. Willis and D. K. Skinner, Solid State Commun. **13**, 685 (1973).
[40]B. N. J. Persson and J. E. Demuth, Phys. Rev. B **30**, 5968 (1984), and references therein.
[41]N. Daude, C. Jouanin, and C. Gout, Phys. Rev. B **15**, 2399 (1977).
[42]J. T. Gourtley and W. A. Ruciman, J. Phys. C **6**, 583 (1973).
[43]C. A. Mead, J. Appl. Phys. **32**, 646 (1961).
[44]F. L. Battye, J. G. Jenkin, J. Liesegang, and R. C. G. Leckey, Phys. Rev. B **9**, 2887 (1974).
[45]A. I. Braunstein, M. Braunstein, and G. S. Picus, Phys. Rev. Lett. **15**, 956 (1965).
[46]J. R. Hayes, A. F. J. Levi, and W. Wiegmann, Electron. Lett. **20**, 851 (1984).
[47]E. J. Ryder, Phys. Rev. **90**, 766 (1953).
[48]N. W. Ashcroft and N. D. Mermin, *Solid State Physics* (Holt-Saunders, New York, 1976), p. 344.
[49]J. Olivier and R. Poirier, Surf. Sci. **105**, 347 (1981).
[50]J. J. Ritsko, J. Chem. Phys. **70**, 5343 (1979).